Strain-assisted bandgap modulation in Zn based II-VI semiconductors

S. K. Yadav and R. Ramprasad[a)]
Chemical, Materials, and Biomolecular Engineering, Institute of Materials Science, University of Connecticut, Storrs, Connecticut 06269, USA

(Received 19 December 2011; accepted 23 May 2012; published online 14 June 2012)

The electronic structure of bulk ZnX (X = O, S, Se, and Te) under uniaxial strain along the [0001] direction or equibiaxial strain along the (0001) plane is investigated using hybrid density functional theory calculations and many-body perturbation theory. It is shown that compressive uniaxial (or tensile equibiaxial) strains lead to a structural phase transition in all the ZnX systems. This is accompanied by large reductions in the bandgap of ZnSe and ZnTe, spanning the entire visible spectrum. © *2012 American Institute of Physics*. [http://dx.doi.org/10.1063/1.4729153]

ZnX (X = O, S, Se, and Te) systems, an important class of benign large bandgap (E^{gap}) semiconductors have been the subject of intense interest because of their potential wide-ranging applications in electronic and optoelectronic devices.[1] A crucial threshold in the usage of ZnX in photocatalysis and photovoltaics is our ability to engineer (i.e., reduce) their E^{gap} to desired values. Doping with various elements has been a popular way to modulate E^{gap} but this approach is limited by the doping ratio.[2] Yet another way to perform such tuning is by applying external stresses (such as hydrostatic pressure) or inducing intrinsic strains through lattice mismatch in epitaxial films or core/shell nanowires. Such lattice mismatch leads to either biaxial strains along the interfacial plane or uniaxial strains normal to the interface plane. Spectacular variations in E^{gap} due to strains have indeed been recently reported for ZnO,[3] CdSe,[4,5] and CdTe (Refs. 4 and 5) nanowires, and ZnX (Ref. 6) and GaN (Refs. 4 and 7) bulk. It is noteworthy that the bandgap variations are accompanied by structural variations in which the equilibrium wurtzite structure (W) transforms to a graphite-like phase (W-G) under compression,[6] reminiscent of a similar phase displayed by ultrathin ZnO films grown on Ag.[8]

All of the above reported E^{gap} trends (and structural phase transformations) were predicted by density functional theory (DFT) calculations using (semi)local exchange-correlation functionals. The well-known E^{gap} underestimation deficiency of conventional DFT arises due to self-interaction errors inherent in the (semi)local treatment, and places uncertainties in the prior predictions. In order to test the veracity of the trends predicted earlier by (semi)local DFT and to provide quantitative estimates of E^{gap} reductions, we use two sophisticated methods in this study: hybrid DFT using the Heyd-Scuseria-Ernzerhof (HSE) hybrid functional,[10] and the *GW* method.[13–15] Hybrid DFT methods based on the HSE scheme are increasing in popularity as they are able to improve the accuracy of E^{gap} predictions of insulators over the (semi)local treatment at an affordable cost.[19] The *GW* method, on the other hand, is based on many-body perturbation theory, and offers a parameter-free option to the accurate prediction of the electronic structure of insulators. These methods are currently the benchmarks for electronic structure calculations, but are also computationally demanding.

In this work, we focus on the bulk ZnX class of systems in the wurtzite structure subjected to uniform uniaxial strains along the [0001] direction (equivalently, equibiaxial strains in (0001) plane). We note that while the ground state structure of ZnO is wurtzite, and that of ZnS, ZnSe, and ZnTe is zinc blende, the energy difference between the wurtzite and zinc blende phases of the latter systems are very small.[6] In fact, the wurtzite form of ZnS,[16] ZnSe,[17] and ZnTe (Ref. 18) have all been observed experimentally. Moreover, our own prior (semi)local DFT work that included a study of ZnX in the zinc blende structure strained along the [111] direction (equivalent to the [0001] direction in the wurtzite structure) provided structural, energetic and electronic structure results similar to that for the wurtzite systems.[6] Hence, for uniformity, we focus primarily on wurtzite ZnX in the present beyond-(semi)local DFT study. We find that the change in the E^{gap} predicted by (semi)local DFT due to the imposed uniaxial strains is in close agreement with the corresponding HSE and *GW* results, although the actual magnitude of the E^{gap} values are significantly underestimated by (semi)local DFT. The previously predicted W to W-G structural phase transformation is also recovered for all cases at the HSE level of theory.

Our calculations were performed using the Vienna *ab initio* simulation package (VASP).[20] Geometry optimizations were done using both (semi)local DFT and hybrid DFT calculations. The DFT calculations employed the Perdew, Burke, and Ernzerhof (PBE)[21] exchange-correlation functional and the projector-augmented wave methodology.[22] The hybrid DFT calculations utilized the specific functional referred to as the HSE06 functional in the literature.[10] This functional is created by starting with the PBE exchange-correlation functional and replacing 25% of the PBE exchange interaction by a screened nonlocal functional with an inverse screening length of 0.2 Å^{-1}. A $7 \times 7 \times 7$ Monkhorst–Pack mesh for k-point sampling and a plane-wave cutoff of 400 eV for the plane wave expansion of the wave functions were used. For each level of imposed uniaxial strain along the [0001] direction, the lattice parameter along the orthogonal direction and the atomic positions were optimized to a high level of accuracy. Fig. 1(a) shows the PBE and HSE optimized geometry versus strain, with the

a)rampi@ims.uconn.edu.

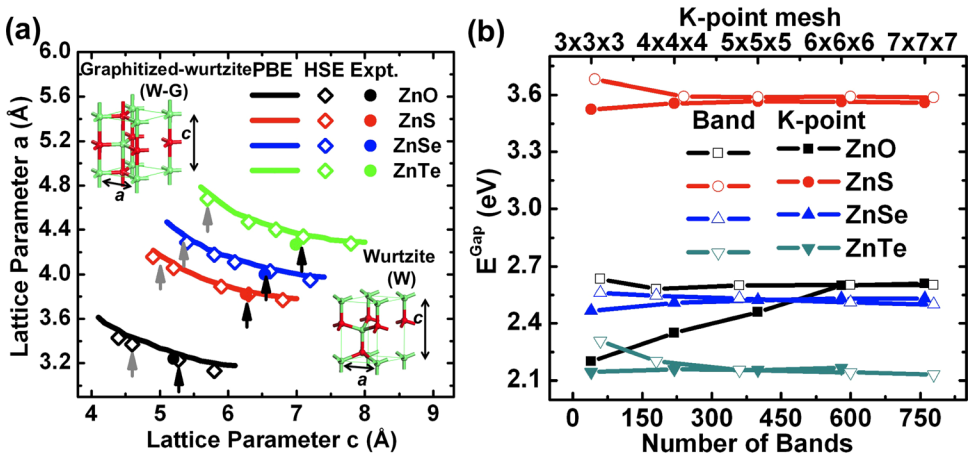

FIG. 1. (a) PBE and HSE optimized a and c lattice parameters. Black and grey arrows indicate, respectively, the equilibrium (W) situation and the point at which the transformation to the W-G phase is complete. Experimental equilibrium a and c lattice parameters are also indicated. (b) G_0W_0-PBE E^{gap} as a function of k-point mesh and number of bands.

equilibrium situation and the completion of the W to W-G phase transformations marked by arrows. Lattice parameters, internal coordinates, and the W to W-G phase transformations calculated by both theories are in excellent agreement with each other. Therefore, subsequent HSE and *GW* calculations used the PBE optimized geometries and did not involve any further optimization.

The starting point for the *GW* calculations was either the PBE wave functions and eigenvalues or the HSE wave functions and eigenvalues. In either case, self-consistency was achieved by iteratively updating both the wave functions and eigenvalues of G and W, leading to the same final result regardless of the starting point; we refer to these results as *scGW*. The first step of this iterative process provided us with the so-called G_0W_0-PBE or G_0W_0-HSE results, depending on the starting point. It is known that the *GW* calculations are sensitive to the number of unoccupied bands and k-points, and that careful checks have to be performed to insure convergence.[20] Fig. 1(b) shows the variation of the G_0W_0-PBE E^{gap} as a function of number of k-points and number of bands for all ZnX systems considered. These results indicate that a $7 \times 7 \times 7$ k-point mesh and 400 bands are required for ZnO and that a $5 \times 5 \times 5$ k-point mesh and 600 bands are sufficient for ZnS, ZnSe, and ZnTe. These parameters were then used in the G_0W_0-HSE and the *scGW* calculations.

Table I lists E^{gap} of ZnX at zero strain predicted at various levels of theory. Available experimental values and the results of prior theory work are also included in Table I. While still underestimating the E^{gap} for all cases relative to experiments, HSE provides a systematically improved prediction relative to PBE. Moving on to the *GW* results, it can be seen that the E^{gap} values are uniformly shifted closer to the experimental values, with the agreement with experiment being better for the G_0W_0-HSE case compared to the G_0W_0-PBE case. It is noteworthy that the *scGW* results are consistently larger than the experimental values for all cases. While these trends are consistent with prior *GW* work,[9,23,25] we note that the discrepancies between our and the prior *GW* work (*cf.* Table I) may be attributed to different k-point meshes and number of bands used in the different studies.

Next, we use the PBE, HSE, G_0W_0-HSE, and *scGW* schemes in our study of the variation of the electronic structure of ZnX with uniaxial strain. Fig. 2 shows the dependence of E^{gap} of ZnX as a function of the lattice parameter (and strain) along the [0001] direction, and the level of theory. Apart from the differences in the actual magnitude of the E^{gap} values predicted at different levels of theory, trends in the E^{gap} variation are consistent between theories. In all cases, modulations in the E^{gap} values due to strain is well captured at the (semi)local level of theory. In the case of ZnO and ZnS, it appears that E^{gap} predicted by different levels of theory are offset by a constant factor. On the other hand, in the case of ZnSe and ZnTe, E^{gap} (computed at higher levels of theory) spans almost the entire visible spectrum in the strain ranges considered. Moreover, in these latter systems, percentage changes in E^{gap} appear to be invariant between theories. (*cf.* Fig. 2).

To investigate the E^{gap} opening at various levels of theory, we consider the position of the band edges with respect to a universal energy reference at the equilibrium geometry. Recent work indicates that the average electrostatic potential provides such a reference appropriate for comparison of energy level positions across different levels of theory.[27,28] Fig. 3 shows the position of the valence band maximum (VBM) and the conduction band minimum (CBM) for each of the ZnX systems as predicted by PBE, HSE, G_0W_0-HSE, and *scGW*. It can be seen that the E^{gap} opening in the case of ZnO and ZnS as we go to higher levels

TABLE I. Comparison of the calculated E^{gap} value of ZnX at various levels of theories with experiments.

System		PBE	G_0W_0-PBE	HSE	G_0W_0-HSE	*scGW*	Expt.
ZnO	This	0.77	2.59	2.46	3.49	3.70	3.40[d]
	Ref.	0.80[a]	2.12[b]	2.50[a]	…	3.80[c]	
ZnS	This	2.08	3.56	3.34	4.08	4.32	3.91[d]
	Ref.	2.07[b]	3.29[b]	…	…	4.15[c]	
ZnSe	This	1.20	2.49	2.35	2.99	3.09	2.71[d]
	Ref.	1.19[e]	…	…	…	…	
ZnTe	This	1.14	2.14	2.13	2.58	2.60	2.39[d]
	Ref.	1.14[e]	…	…	…	…	

[a]Ref. 25.
[b]Ref. 9.
[c]Ref. 23.
[d]Ref. 11.
[e]Ref. 12.

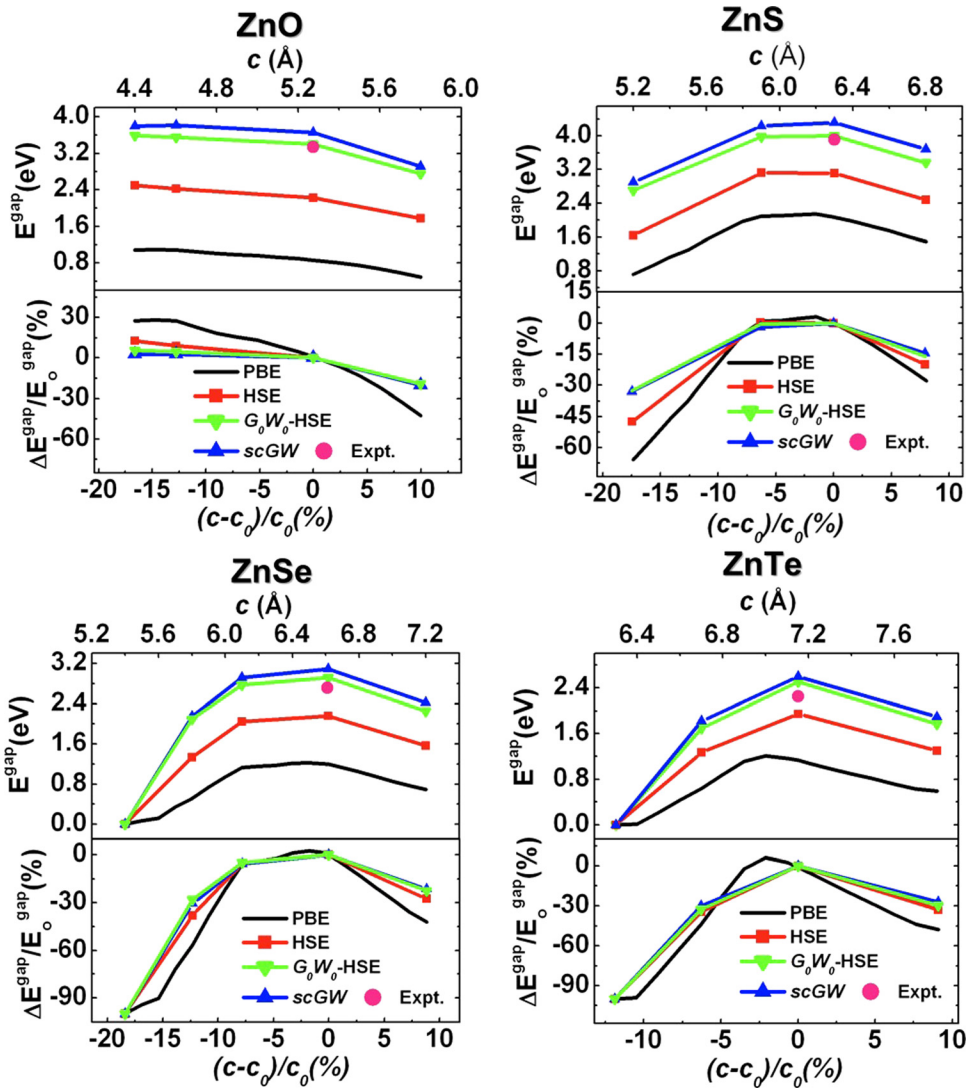

FIG. 2. Absolute (top panel) and relative (lower panel) values of the E^{gap} calculated using PBE, HSE, G_0W_0-HSE, and *scGW* as a function of lattice parameter c and strain, respectively. Symbols represent the actual calculated values and the lines are guides to the eye. Experimental values at equilibrium are also indicated.

of theory is dominated by the lowering of the VBM, while both the VBM and CBM movements contribute to the E^{gap} opening roughly equally in the case of ZnSe and ZnTe.

In order to ascertain that strain-dependent electronic structure features other than the E^{gap} are also well captured by (semi)local DFT, we consider the band structure of ZnTe at equilibrium and two levels of uniaxial strain (−6.3% and 9%) at the PBE, HSE, and *scGW* levels of theory in Fig. 4. The zero of energy is set to the VBM. We note that the DFT band structure at equilibrium (i.e., at 0% strain) computed here is in excellent agreement with prior work.[24] The bands in the valence band manifold as predicted by the three levels of theory are in near-perfect agreement. Moreover, the bands of the conduction band manifold preserve their shape between theories and are just rigidly offset from each other. A similar rigid shift of bands has been reported for equilibrium ZnO as calculated by HSE (Ref. 25) and *GW*.[26]

In conclusion, the impact of uniaxial strains along the [0001] axis on Zn*X* systems has been critically assessed using hybrid DFT and many body *GW* calculations. Our

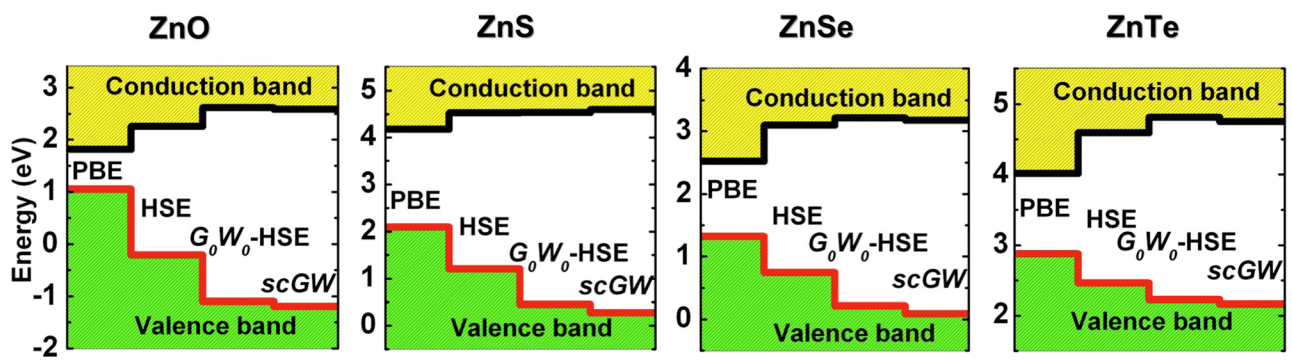

FIG. 3. Positions of the VBM and the CBM at different levels of theory at the equilibrium geometry.

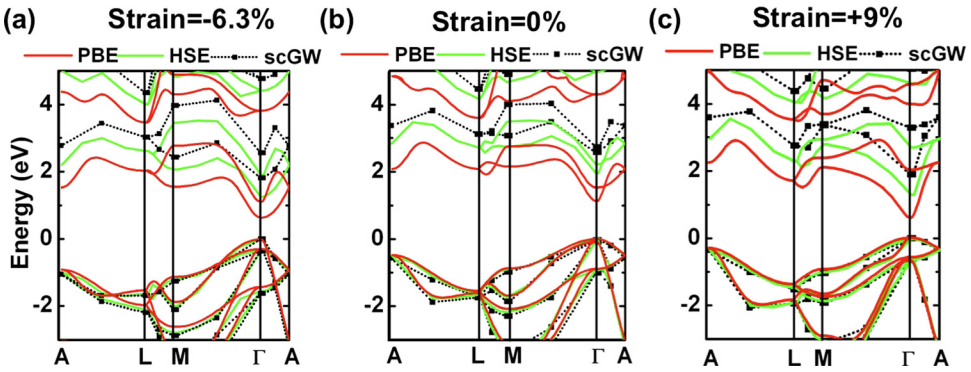

FIG. 4. Band structure of ZnTe at uniaxial strains of −6.3% (a), 0% (b), and 9% (c), calculated using PBE, HSE, and *scGW*.

results confirm the trends identified earlier based on conventional (semi)local DFT calculations which are notorious in underestimating the bandgaps of insulators. In particular, the structural phase transformation of wurtzite Zn*X* to graphite-like Zn*X* under uniaxial compression persists at the hybrid DFT level of theory, and the concomitant significant reduction of the bandgap due to strain in ZnSe and ZnTe is reaffirmed by both the hybrid DFT and *GW* methods. It is hoped that the present findings will stimulate complementary experimental work, to fully exploit the possibilities underlying the bandgap engineering of Zn*X* systems through strain.

Financial support of this work through a grant from the National Science Foundation (NSF) and computational support through a NSF Teragrid Resource Allocation are acknowledged. Helpful discussions with Patrick Rinke are also acknowledged.

[1]S. Adachi, *Properties of Semiconductor Alloys: Group-IV, III-V and II-VI Semiconductors* (Wiley, United Kingdom, 2009).
[2]S. B. Zhang, S.-H. Wei, and A. Zunger, Phys. Rev. Lett. **84**, 1232 (2000).
[3]J. Schrier, D. O. Demchenko, L.-W. Wang, and A. P. Alivisatos, Nano Lett. **7**, 2377 (2007).
[4]S. Yang, D. Prendergast, and J. B. Neaton, Nano Lett. **10**, 3156 (2010).
[5]T. Sadowski and R. Ramprasad, J. Phys. Chem. C **114**, 1773 (2010).
[6]S. K. Yadav, T. Sadowski, and R. Ramprasad, Phys. Rev. B **81**, 144120 (2010).
[7]L. Dong, S. K. Yadav, R. Ramprasad, and S. P. Alpay, Appl. Phys. Lett. **96**, 202106 (2010).
[8]C. Tusche, H. L. Meyerheim, and J. Kirschner, Phys. Rev. Lett. **99**, 026102 (2007).
[9]M. Shishkin and G. Kresse, Phys. Rev. B **75**, 235102 (2007).
[10]A. Krukau, O. Vydrov, A. Izmaylov, and G. Scuseria, J. Chem. Phys. **125**, 224106 (2006).
[11]S. O. Kasap and P. Capper, *Springer Handbook of Electronic and Photonic Materials* (Springer, Canada, 2006).
[12]J. Heyd, J. E. Peralta, and G. E. Scuseria, J. Chem. Phys. **123**, 174101 (2005).
[13]L. Hedin, Phys. Rev. **139**, A796 (1965).
[14]F. Oba, A. Togo, I. Tanaka, J. Paier, and G. Kresse, Phys. Rev. B **77**, 245202 (2008).
[15]A. Stroppa and G. Kresse, Phys. Rev. B **79**, 201201(R) (2009).
[16]C. Ma, D. Moore, J. Li, and Z. L. Wang, Adv. Mater. **15**, 228 (2003).
[17]A. B. Panda, S. Acharya, and S. Efrima, Adv. Mater. **17**, 2471 (2005).
[18]J. Zhang, S. Jin, H. C. Fry, S. Peng, E. Shevchenko, G. P. Wiederrecht, and T. Rajh, J. Am. Chem. Soc. **113**, 15324 (2011).
[19]T. M. Henderson, J. Paier, and G. E. Scuseria, Phys. Status Solidi B **284**, 767 (2011).
[20]G. Kresse and J. Furthmuller, Phys. Rev. B **54**, 11169 (1996).
[21]J. P. Perdew, K. Burke, and M. Ernzerhof, Phys. Rev. Lett. **77**, 3865 (1996).
[22]P. E. Blöchl, Phys. Rev. B **50**, 17953 (1994).
[23]M. Shishkin, M. Marsman, and G. Kresse, Phys. Rev. Lett. **99**, 246403 (2007).
[24]O. Zakharov, A. Rubio, X. Blase, M. L. Cohen, and S. G. Louie, Phys. Rev. B **50**, 10780 (1994).
[25]J. Wróbel, K. J. Kurzydlowski, K. Hummer and G. Kresse, and J. Piechota, Phys. Rev. B **80**, 155124 (2009).
[26]T. Kotani, M. van Schilfgaarde, and S. V. Faleev, Phys. Rev. B **76**, 165106 (2007).
[27]R. Ramprasad, H. Zhu, P. Rinke, and M. Scheffler, Phys. Rev. Lett. **108**, 066404 (2012).
[28]A. Alkauskas and A. Pasquarello, Phys. Rev. B **84**, 125206 (2011).